J Mater Sci (2010) 45:4571–4577
DOI 10.1007/s10853-010-4552-y

ULTRAFINE GRAINED MATERIALS

Information on deformation mechanisms in nanocrystalline Pd–10% Au inferred from texture analysis

Yu. Ivanisenko · W. Skrotzki · R. Chulist · T. Lippmann · K. Yang · L. Kurmanaeva · H.-J. Fecht

Received: 9 February 2010 / Accepted: 16 April 2010 / Published online: 7 May 2010

Abstract There is still a lack of understanding of deformation mechanisms in nanocrystalline (nc) materials. Studies on microstructures formed in nc Pd–10% Au (grain size about 15 nm) after high pressure torsion revealed signatures of various deformation processes as cooperative grain boundary sliding (GBS), shear banding, dislocation slip and twinning. In order to estimate contributions of these processes to total strain, a comparison was made between torsion textures formed in nc and coarse grained (cg) samples after identical shear strain. The textures were measured with synchrotron radiation. Intensities of characteristic components of the shear texture are two times stronger in the cg sample than in the nc one, indicating that dislocation slip is less significant in the nc sample. It is proposed that numerous planes of cooperative GBS revealed by TEM contribute to plasticity of nc alloy.

Yu. Ivanisenko (✉) · L. Kurmanaeva · H.-J. Fecht
Institut für Nanotechnologie, Karlsruher Institut für Technologie (KIT), 76021 Karlsruhe, Germany
e-mail: julia.ivanisenko@kit.edu

W. Skrotzki · R. Chulist
Institut für Strukturphysik, Technische Universität Dresden, 01062 Dresden, Germany

T. Lippmann
Institut für Werkstoffforschung, GKSS Forschungszentrum Geesthacht, 21502 Geesthacht, Germany

K. Yang · H.-J. Fecht
Institut für Mikro- und Nanomaterialien, Universität Ulm, 89081 Ulm, Germany

Introduction

Understanding of deformation mechanisms operating in nanocrystalline (nc) materials is very important to predict their mechanical properties and is necessary for scientifically justified design of new materials. The mechanical behaviour of nc materials differs from that of coarse-grained (cg) ones for a number of reasons including the difficulty of nucleating and propagating dislocations [1–3] and the consequent emergence of alternative deformation mechanisms including grain boundary sliding (GBS) [3], diffusional creep [3, 4], emission of partial dislocations from grain boundaries [3] and mechanical twinning [5–8]. The results collected until now are controversial, on the one hand, theoretical considerations [9], MD simulations [3] and some experiments [8, 10] favour grain boundary mediated processes, on the other hand, very low ductility and relatively low strain rate sensitivity (order of 0.05) typically revealed in nc metals point towards dislocation mediated mechanisms [11–14]. Analysis of the texture formed during plastic deformation could be very helpful to estimate the contributions to strain of various deformation mechanisms, because such processes like dislocation slip and mechanical twinning occurring in specific crystallographic planes lead to preferred orientations depending on different factors like staking fault energy, temperature of deformation and others. On the other hand, in general GBS leads to randomization of the existing texture. Texture analysis has been frequently used in studies of conventional superplastic straining [15, 16], and several such attempts were also undertaken recently in nc materials [17, 18].

The ductility of nc metals and alloys in conventional mechanical tests is usually limited to just several percents, which makes subsequent texture measurements almost

useless. In contrast, the recently developed method of mechanical testing by torsion under high pressure (instrumented high pressure torsion, HPT) allows achieving practically unlimited strains without fracture of the specimen [8, 19]. Here, a report is given on synchrotron measurements of texture development as a result of HPT of nc and cg specimens of the Pd–10% Au alloy with initial random texture. As revealed by previous investigations [8] strong grain growth took place in nc Pd deformed in HPT to large strains. Therefore, the present study was limited to shear strains of 15–20. Microstructure investigations confirmed that up to this value the mean grain size in the nc samples remained below 30 nm.

Experimental

Nanocrystalline (nc) Pd–10 at.% Au powder was produced by inert gas condensation (igc) [20] using a 10^{-7} mbar base pressure vacuum system and thermal evaporation of Pd (99.95%) and Au (99.95%) in a 1 mbar helium atmosphere. The powder was consolidated in situ at a pressure of 2 GPa to obtain disc-shaped specimens with a diameter of 8 mm and thickness of typically 0.3 mm. It is worth noting that nc Pd–10 at.% Au samples exhibit a stable grain size even at temperatures well above ambient, in contrast to pure nc Pd where rapid grain coarsening was observed at room temperature [21]. As reference, a cg Pd–10% Au specimen produced by annealing with a mean grain size of 100 μm and the same dimensions as the nc sample was also deformed by HPT.

Quasi-hydrostatic HPT was conducted under a pressure of 4.5 GPa in a Schenck^{TM} testing machine with an axial load capacity of 400 kN. All samples were twisted at a constant rotation rate of $\pi/2$ per 18 s.

Disc-shaped specimens (diameter 3 mm) for transmission electron microscopy (TEM) were taken at approximately 3 mm from the centre of the HPT samples. They were mechanically grounded and dimpled, and then further thinned to a thickness of electron transparency using a Gatan Precision Ion Polishing System (PIPS, Gatan, USA) with Ar^+ ions accelerated at 2.5–3.5 kV. The shear strain, γ, corresponding to 3 mm from the centre of the disc after a rotation of $\pi/2$ is: $\gamma = \frac{\pi r}{2t} = 21 (r = 3$ mm, distance from centre; $t = 0.2$ mm, thickness of disc after HPT) dark field images were taken with a Phillips CM 30 operated at 300 kV.

Coarse-grained (cg) Pd–10% Au samples were investigated by orientation imaging microscopy (OIM) in a scanning electron microscope (FEG-SEM) LEO 1550 operated at 25 kV and INCA Crystal software (Oxford Instruments) was used for indexing the electron back scattering diffraction (EBSD) patterns. The scanning step size corresponds to a pixel size, which was 0.1 × 0.1 μm. The error in the determination of the crystallographic orientation of each grain was less than 3°. The analysis was performed for approximately 500 grains mapped in 3–5 OIM scans for each sample. Boundaries with misorientation angle less than 2° were neglected. The as-obtained OIM maps were subjected to a 'cleaning' procedure, where single unsolved pixels were filled with the value from its nearest neighbours. A group of unsolved pixels is not changed in this procedure. The average grain size (i.e. equivalent diameter) was estimated from the 'cleaned' grain maps, from which the amount of pixels corresponding to the areas with the same crystallographic orientation and surrounded by grain boundaries with a threshold value of 15° was counted.

For local texture measurements, small pins (1.5 mm × 0.2 mm × 10 mm) were cut by spark-erosion from the disc-shaped specimens in radial direction as shown in Fig. 1. Quantitative texture measurements in a 0.15 mm^3 volume of the pin located at app. 2.1 mm from the centre of the disc corresponding to a shear strain of 15 ± 0.7 were performed with high energy (100 keV synchrotron radiation at beamline HARWI II at DESY-HASYLAB, Hamburg, Germany). A detailed description of the synchrotron texture measurement is given in [22]. The orientation distribution function (ODF) was calculated on the basis of the

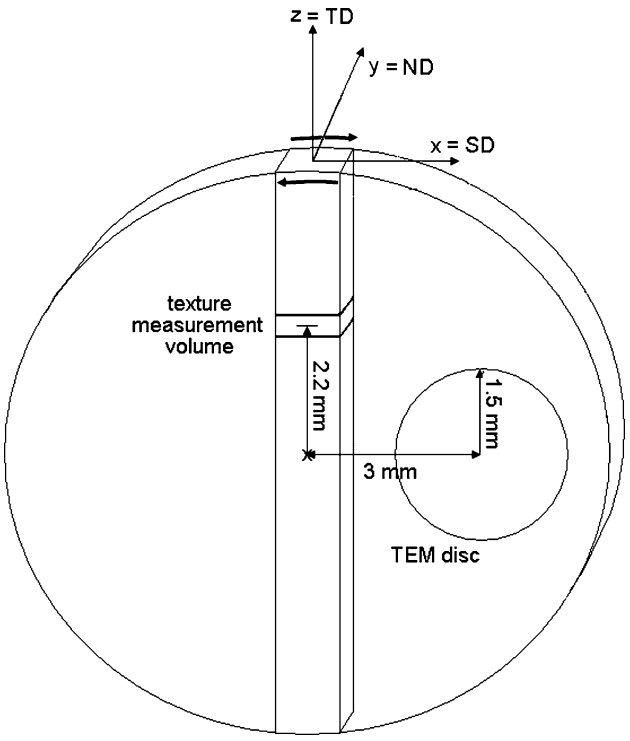

Fig. 1 Schematic diagram showing how pins for texture measurements and 3 mm TEM discs were cut by spark-erosion from the HPT specimens

measured (111), (200) and (220) pole figures using LABOTEX software [23]. The Euler angles were used in Bunge notation [24]. To account best for the monoclinic symmetry of simple shear, the crystal and sample reference systems have been defined as X||shear direction (SD), Y||shear plane normal (ND), Z||transverse direction (TD) [25]. The textures are represented by $\varphi_2 = 0°$ and $\varphi_2 = 45°$ ODF sections, which for face-centred cubic (FCC) metals contain all major shear components (Table 1).

Results

The typical torque against twist angle curves for cg and nc samples are shown in Fig. 2. The torque in coarse grain sample increases almost linearly with the increasing of the twist angle, whereas nc igc sample shows rapid strain hardening in the beginning of straining which almost levels out after rotation for app. 30°.

Table 1 Ideal texture components in simple shear [27] observed in cg and nc Pd–10% Au specimens after HPT deformation and corresponding ODF intensities

Component designation	Miller indices (hkl)||shear plane, [uvw]||shear direction	Intensity, m.r.d.	
		nc	cg
A	$(11\bar{1})[1\bar{1}0]$	1.4	1.2
$\overline{A}$	$(\bar{1}\bar{1}1)[\bar{1}10]$	1.4	1.2
B	$(11\bar{2})[1\bar{1}0]$	2.4	2.7
$\overline{B}$	$(\bar{1}\bar{1}2)[\bar{1}10]$	2.3	2.8
C	$(100)[0\bar{1}1]$	0.9	4.1
A_1^*	$(11\bar{1})[2\bar{1}1]$	1.0	1.1
A_2^*	$(1\bar{1}1)[\bar{2}\bar{1}1]$	2.6	2.2
Cube	(001)[100]	2.0	–

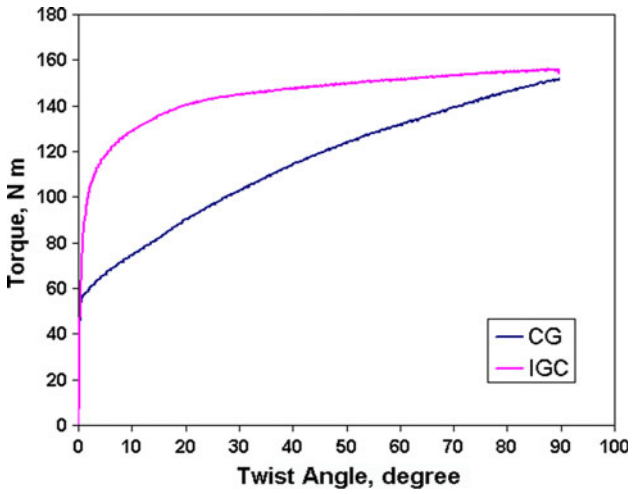

Fig. 2 Torque against twist angle curves of coarse crystalline (cg) and nc (igc) Pd–10% Au alloy (Color figure online)

The as-igc microstructure is very homogeneous (Fig. 3a) with a comparatively narrow grain size distribution (Fig. 3b). The mean grain size as estimated from separate histograms of several TEM micrographs is about 13 nm. Careful inspection revealed only very few twins in the as-igc microstructure. Dislocations can be observed only in a small fraction of grains. Triple points exhibit angles near 120°, as in an equilibrated grain microstructure.

The TEM micrographs of Fig. 3c reveal a larger grain size after HPT. In fact, the histogram of Fig. 2d yields a mean grain size of about 24 nm. It is also seen that the size distribution has broadened (Fig. 3d). With an aspect ratio of 1.1 the grains appear still equiaxed at this high shear strain. Previously, the microstructure of HPT-processed pure igc Pd showed much stronger grain growth after such shear strain as the mean grain diameter increased up to 40 nm [8]. Similarly to pure Pd [8], thin twin lamellae are also observed in many grains, their density is visibly larger than that in the as-igc state.

Present TEM investigations also revealed the formation of planes of cooperative GBS sliding, observed previously in nc Pd [8]. Figure 4 represents examples of such mesoscopic shear planes (indicated with white arrows), which appear as straight lines formed by segments of grain boundaries of adjacent grains. It is seen in the image that angles of traces of boundaries at triple junctions of grains on both sides of such shear planes are straightened to form a line.

For comparison reason, microstructure of coarse crystalline alloy was observed before and after HPT using OIM. Application of OIM was impossible in case of nc alloy due to very small grain size in these samples, however, it is much more convenient than TEM, as it readily provides quantitative information about the mean grain size and grain boundary misorientation parameters. OIM maps showing the spatial distribution of grain boundaries of different types for both conditions of cg samples are presented in Fig. 5a, b. In the initial state the mean distance between the boundaries with a misorientation angle >15° (diameter of the similarly oriented volumes) is about 100 μm. HPT leads to significant reduction of this distance to 315 nm. OIM also allows to distinguish special grain boundaries from the random ones. The GB types are classified according to CSL-theory using the proximity (or Brandon) condition of $\Delta\theta = 15°\Sigma^{-1/2}$ [26]. In this notation, twin boundaries are designated as Σ3, and they are shown in Fig. 5b with yellow colour. It can be seen that several twin boundaries are present in the image.

The initial texture of the as-igc Pd–10% Au specimens is practically random with an orientation density stochastically varying between 1 and 2 m.r.d (multiples of a random

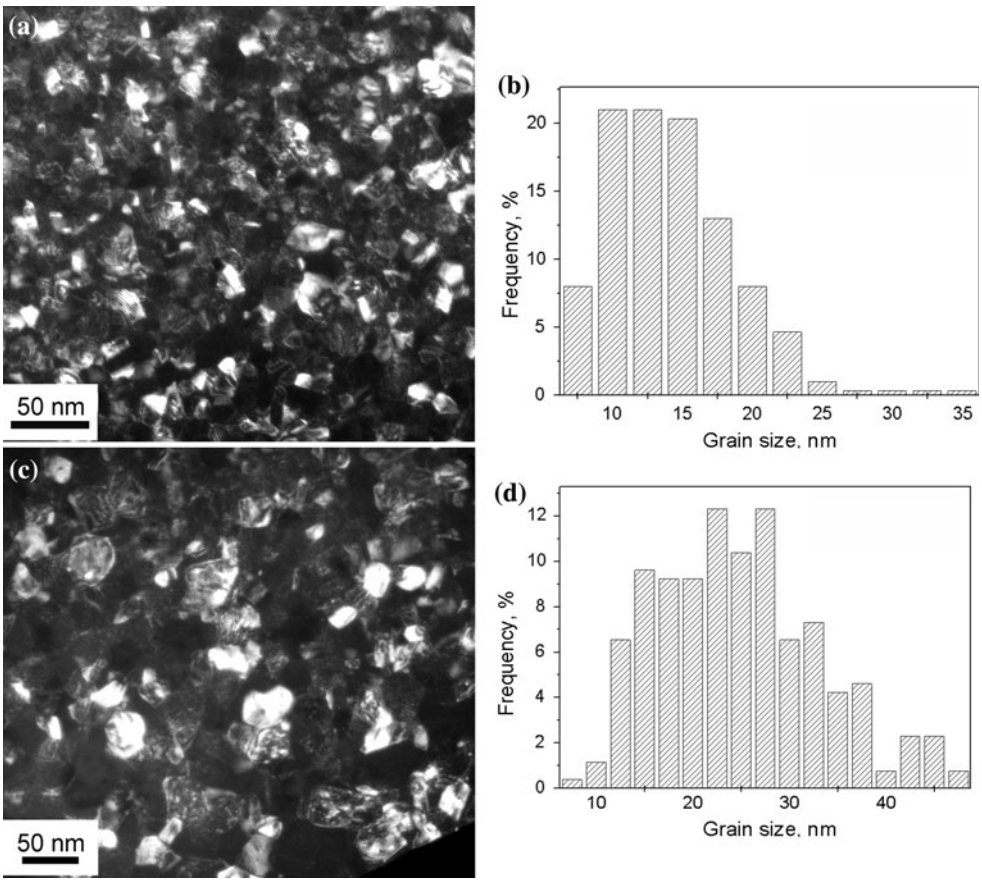

Fig. 3 Typical dark field TEM images of the microstructure (**a**, **c**) and corresponding grain size distribution histograms (**b**, **d**) of nc Pd–10% Au alloy: **a**, **b** as-igc microstructure, v**c**, **d** after subsequent HPT straining at $\gamma = 20$ (image plane = HPT disc plane)

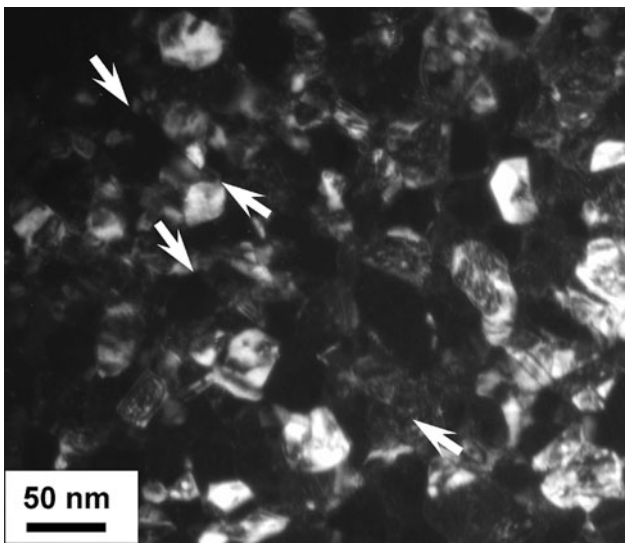

Fig. 4 Dark field TEM image showing typical examples of cooperative shear planes (marked by *white arrows*) in HPT-processed nc Pd–10% Au alloy. These planes represent almost straight lines built by boundary segments of several adjacent grains with straightened triple points (image plane = disc plane)

distribution), (Fig. 6). Due to poor grain statistics in the cg specimen, it was difficult to analyze the initial texture quantitatively. However, it seems to be also random.

Figure 1 represents the geometry of HPT deformation: shear plane is parallel to the disc plane, and shear direction is normal to the specimen radius. It is known that simple shear textures of FCC metals are characterized by two partial fibres: (i) $\{111\}\|\mathrm{ND}$ containing $A/\overline{A}, A_1^*, A_2^*$ ideal components and (ii) $\langle 110\rangle\|\mathrm{SD}$ containing $A/\overline{A}, B/\overline{B}$ and C ideal components [27]. Crystallographic indices of the ideal components are given in Table 1. Figure 5 represents the $\varphi_2 = 0°$ and $\varphi_2 = 45°$ ODF sections of HPT-processed nc and cg samples. The positions of simple shear ideal orientations for the respective ODF sections are indicated in the key figure of Fig. 6. As it is seen in Fig. 6, the texture characteristic for simple shear develops in both samples after HPT deformation, but the intensities of typical texture components generally are stronger in the cg sample as compared with the nc one (Table 1). It is worth noting that in nc Pd–10% Au the strongest component is A_2^*, whereas in the cg alloy this is C.

Additionally, a relatively strong oblique cube component $\{100\}\langle 100\rangle$ is present in the nc specimen (Fig. 6; Table 1). This texture typically forms in FCC metals during recrystallization, but here it appears more likely as a result of stress-induced grain growth [8] and not due to static recrystallization as samples exhibit a stable grain size even at temperatures well above ambient.

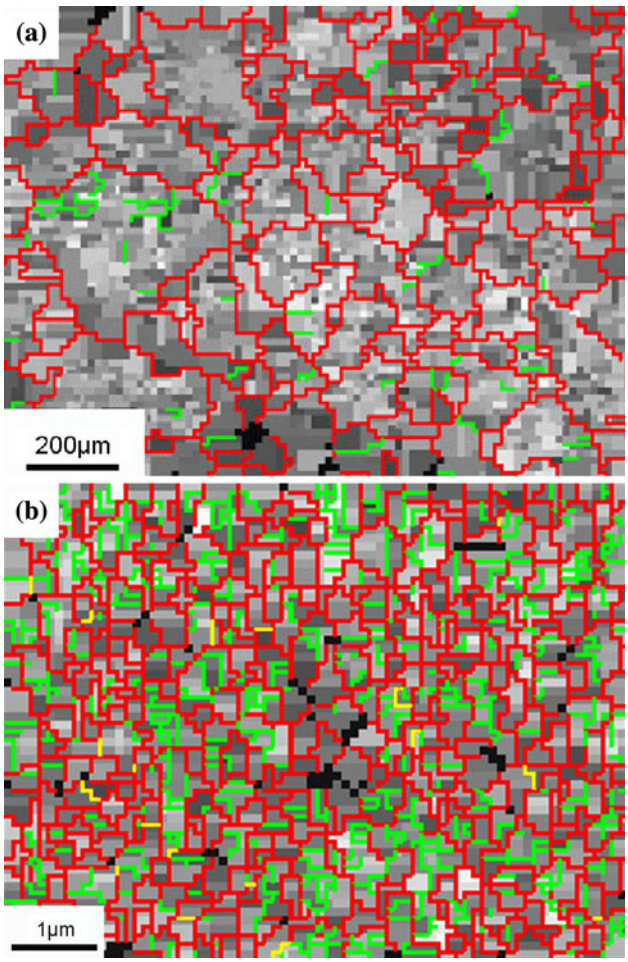

Fig. 5 Spatial distributions of different boundary types produced by orientation imaging microscopy: **a** annealed state, and **b** after subsequent HPT straining at $\gamma = 20$ (image plane = HPT disc plane). Grain boundaries with misorientation angles $\geq 15°$ are shown in *red/dark gray*, and these with misorientation angles $<15°$ are shown in *green/light gray*. $\Sigma 3$ boundaries are shown in *yellow/light gray*. Areas that are not indexed are shown in *black* (Color figure online)

Discussion

The strain versus torque graphs of the nc as compared to the initially cg Pd–10% Au alloy look very different (Fig. 2). Conventional cg materials demonstrate a gradual increase of torque until the steady-state is achieved, which corresponds to a dynamic equilibrium for dislocation emission and absorption [19, 28, 29]. This process concurs with grain refinement. Typically, torque and hardness saturate simultaneously with the grain size, and the Hall-Petch law applies. This phenomenology applies during the formation of ultrafine grained materials by severe plastic deformation of initially cg metals. For the initially nanostructured material, our data suggest a quite different behaviour with (i) work hardening only during the very beginning of deformation, and a subsequent stagnation of flow stress, and (ii), stress-induced grain growth rather than grain refinement. The mechanism of strain hardening in nc material where dislocation storage is difficult is not clear yet. TEM observations revealed an increased density of twins, and texture measurements point towards extensive twin formation (see below), this can be a most probable reason for strain hardening. The experimental study of mechanisms of strain hardening in nc $Pd_{90}Au_{10}$ alloy is in process now and will be published separately.

The results obtained reveal the formation of a weak simple shear texture with maximum intensity of 2.6 m.r.d. corresponding to the A_2^* component in a nc specimen of Pd–10% Au alloy with initial random texture. This clearly demonstrates that dislocation slip is active in nc alloys even at such a small grain size. However, the comparison with the cg alloy deformed at the same conditions (Fig. 2) indicates that the contribution of dislocation slip to strain is much less in the nc alloy. The lower intensity of texture points towards a significant contribution of GBS in the deformation process. Some dislocation activity is not surprising as in conventional superplasticity dislocation slip always accompanies GBS. For example, texture measurements on Zn–Al alloy after superplastic straining not only revealed an overall reduction of texture but also a retention of some particular texture components, which is explained by a small amount of slip in isolated grains [15, 16].

TEM investigations of the microstructure of nc Pd–10% Au alloy (Fig. 4) revealed planar grain boundary features interpreted as mesoscopic shear planes, which are clear signatures of cooperative GBS. Cooperative GBS was frequently observed in conventional superplastic flow [e.g. [30] and refs. in it]. It had long been predicted on theoretical grounds that this mechanism of accommodation of steric hindrances should be very important in nc materials at room temperature conditions when diffusion accommodation is impossible [9]. It is worth to mention that macroscopic shear bands frequently observed in ultrafine grained materials [31, 32] were not revealed after careful investigation of the nc microstructure. Grains remain equiaxed (Fig. 3b), and dislocation density after HPT deformation is very low.

It is also worth to noting that the intensity of the $B, \overline{B}$ and A_2^* components, usually observed in torsion textures of low stacking fault materials [33–35] and related to deformation twinning, are relatively strong both in nc and cg specimens (Table 1) in agreement with TEM and EBSD measurements. The stacking fault energy of the Pd–10% Au alloy is 150 mJ/m^2.[1] This is a high enough value which does not allow to expect twinning at conventional

[1] Estimated using embedded atom method (EAM) potentials, unpublished result, courtesy of K. Albe.

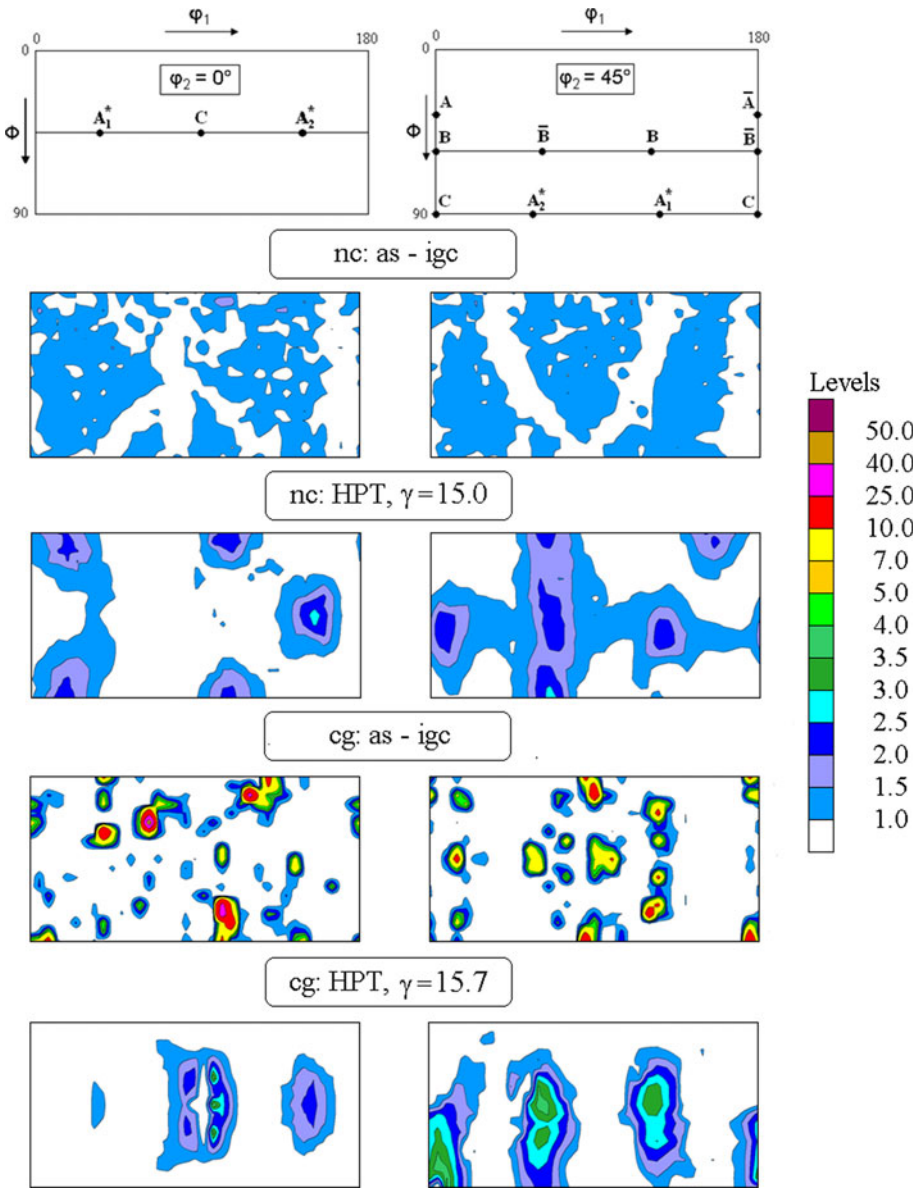

Fig. 6 $\varphi_2 = 0°$ and $\varphi_2 = 45°$ ODF sections of nc and cg samples processed by HPT at 4.5 GPa for shear strains of 15 and 15.7, respectively (Color figure online)

deformation of this alloy. In nc and ultrafine grained state, however, this may be well possible due to a high flow stress exceeding the critical twinning stress [36, 37]. For example, deformation twins were observed in Cu when the grain size as a result of HPT deformation was reduced to some critical value [37]. Anyway, it is clear that mechanical twinning in FCC metals with a shear of 0.71 can only contribute to strain in the order of 15.

TEM investigations of the microstructure changes resulting from HPT in the nc Pd–10% Au alloy confirmed stress-induced grain growth typically observed in nc metals [8, 17, 38]. The development of the characteristic recrystallization cube texture indicates that grain coarsening during HPT more likely does not occur via grain coalescence proposed in [39], but develops through stress-induced grain growth with preferential migration of boundaries of grains with cube orientation [40].

Conclusions

Texture development in coarse crystalline and nc Pd–10% Au alloy as a result of high pressure torsion deformation was studied using synchrotron radiation. It was revealed that a typical shear texture was formed in both specimens, however, the intensity of particular texture components was notably lower in the nc one. This points towards a limited contribution of dislocation slip to plastic deformation of nc alloy and indicates the activation of GBS. The latter was confirmed by TEM observations, which revealed

numerous planes of cooperative GBS in the microstructure. Typical recrystallization cube texture was also found in nc specimen, in agreement with the observation of stress-induced grain growth.

Acknowledgements Funding by the Deutsche Forschungsgemeinschaft (grant FOR 714) is gratefully acknowledged. Authors are thankful to Dr. Jürgen Markmann from Universität des Saarlandes, Technische Physik, for providing the nc specimens, to IMF II for access to compression-torsion machine Schenk and Mr. St. Knaak for help in conducting the HPT experiments.

References

1. Karch J, Birringer R, Gleiter H (1987) Nature 330:556
2. Chokshi AH, Rosen A, Karch J, Gleiter H (1989) Scripta Metall 23:1679
3. Van Swygenhoven H (2002) Science 296:66
4. Wolf D, Yamakov V, Phillpot SR, Mukherjee AK, Gleiter H (2005) Acta Mater 53:1
5. Chen MW, Ma E, Hemker KJ, Sheng HW, Wang YM, Cheng XM (2003) Science 300:1275
6. Yamakov V, Wolf D, Phillpot SR, Mukherjee AK, Gleiter H (2002) Nat Mater 1:45
7. Rösner H, Markmann J, Weissmüller J (2004) Philos Mag Lett 84:321
8. Yu I, Kurmanaeva L, Weissmueller J, Yang K, Markmann J, Rösner H, Scherrer T, Fecht H-J (2009) Acta Mater 57:3391
9. Hahn H, Mondal P, Padmanabhan KA (1997) Nanostruct Mater 9:603
10. Shan Z, Stach EA, Wiezorek JMK, Knapp JA, Follstaedt DM, Mao SX (2004) Science 305:654
11. Kumar KS, Van Swygenhoven H, Suresh S (2003) Acta Mater 51:5743
12. Dalla Torre F, Spatig P, Schaublin R, Victoria M (2005) Acta Mater 53:2337
13. Li YJ, Mueller J, Höppel HW, Göken M, Blum W (2007) Acta Mater 55:5708
14. Wang MYM, Hamza AV, Ma E (2006) Acta Mater 54:2715
15. Melton KN, Edington JW, Kallend JS, Cutler CP (1974) Acta Metall 22:165
16. Cutler CP, Edington JW, Kallend JS, Melton KN (1974) Acta Metall 22:665
17. Liao XZ, Kilmametov AR, Valiev RZ, Gao H, Li X, Mukherjee AK, Bingert JF, Zhu YT (2006) Appl Phys Lett 88:021909
18. Kulovits A, Mao SX, Wiezorek JMK (2008) Acta Mater 56:4836
19. Pippan R, Wetcher F, Hafok M, Vorhauer A, Sabirov I (2006) Adv Eng Mater 8(11):1046
20. Birringer R, Gleiter H, Klein H-P, Marquardt P (1984) Phys Lett 102A:365
21. Ames M, Markmann J, Karos R, Michels A, Tschöpe A, Birringer R (2008) Acta Mater 56:4255
22. Skrotzki W, Klöden B, Tamm R, Oertel C-G, Garbe U, Rybacki E (2003) Textures Microstruct 35:163
23. Pawlik K, Ozga P (1999) Göttinger Arb Geol Paläont SB4:146
24. Bunge HJ (1993) Texture analysis in materials science. Mathematical methods. Culliver Verlag, Göttingen
25. Tóth LS, Molinari A (1994) Acta Metall Mater 42:2459
26. Brandon DG (1966) Acta Metall 30:1479
27. Bacroix B (1986) PhD Thesis, McGill University, Montreal
28. Vorhauer A, Pippan R (2008) Metall Mater Trans A39:417
29. Zehetbauer M, Seumer V (1993) Acta Metall Mater 41:577
30. Zelin MG, Mukherjee AK (1995) Acta Metall Mater 43:2359
31. Jia D, Ramesh KT, Ma E (2003) Acta Mater 51:3495
32. Hayes RW, Witkin D, Zhou F, Lavernia EJ (2004) Acta Mater 52:4259
33. Bacroix B, Jonas JJ (1988) In: Kallend JS, Gottstein G (eds) Proceedings of the 8th international conference on textures of materials (ICOTOM 8). The Metallurgical Society, Warrendale, PA, p 403
34. Skrotzki W, Scheerbaum N, Oertel C-G, Brokmeier H-G, Suwas S, Tóth LS (2005) Mater Sci Forum 495–497:821
35. Beyerlein IJ, Tóth LS, Tome C, Suwas S (2007) Philos Mag 87:885
36. Liao XZ, Zhou F, Lavernia EJ, Srinivasan SG, Baskes MI, He DW, Zhu YT (2003) Appl Phys Lett 83:632
37. Liao XZ, Zhao YH, Zhu YT, Valiev RZ, Gunderov DV (2004) J Appl Phys 96:636
38. Gianola DS, Van Petegem S, Legros M, Brandstetter S, Van Swygenhoven H, Hemker KJ (2006) Acta Mater 54:2253
39. Wang YB, Ho JC, Liao XZ, Li HQ, Ringer SP, Zhu YT (2009) Appl Phys Lett 94:011908
40. Humphreys FJ, Hatherly M (2004) Recrystallisation and related annealing phenomena. Elsevier, Oxford, p 406